Figures of Chapter 4, Li_2O

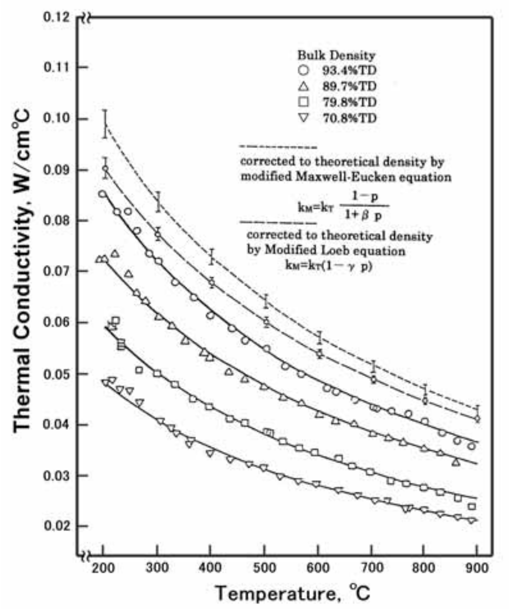

Fig.4.1 Thermal conductivity data for porous Li_2O. [11)]

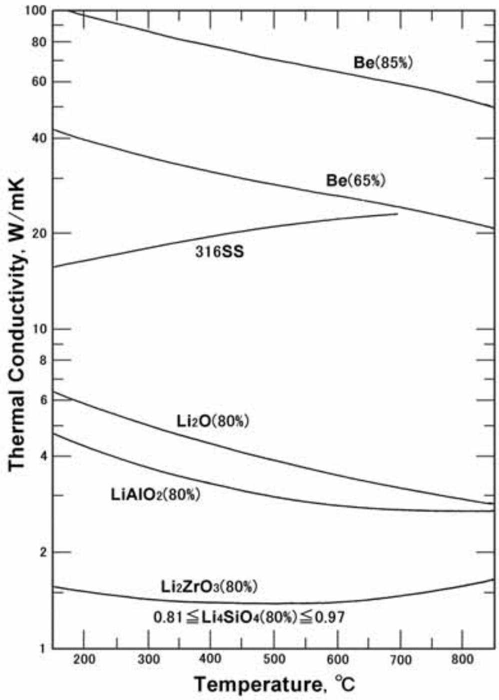

Fig.4.2 Thermal conductivities for Li_2O, Li_2ZrO_3, Li_4SiO_4, Be and 316 SS. [7)]

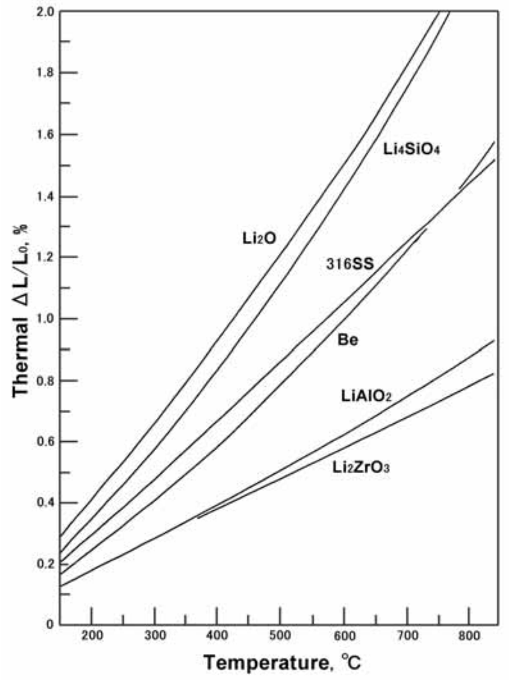

Fig.4.3 Linear thermal expansion strain (referenced to 25 ℃) for Li_2O, Li_2ZrO_3, Li_4SiO_4, Be and 316SS. [10)]

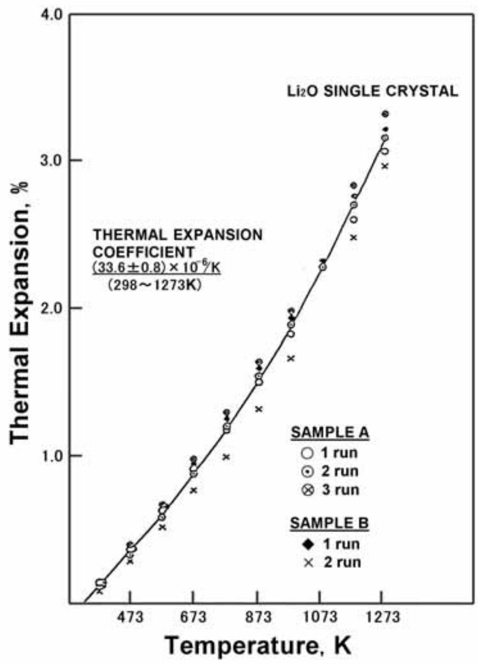

Fig.4.4 Thermal expansion of single crystalLi_2O. [9)]

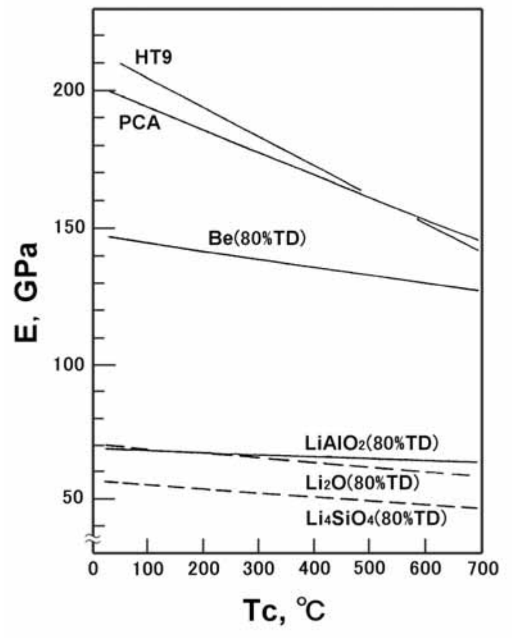

Fig.4.5 Young's Modulus values for Li_2O, Li_4SiO_4, Be, PCA and HT9. [10) 6)]

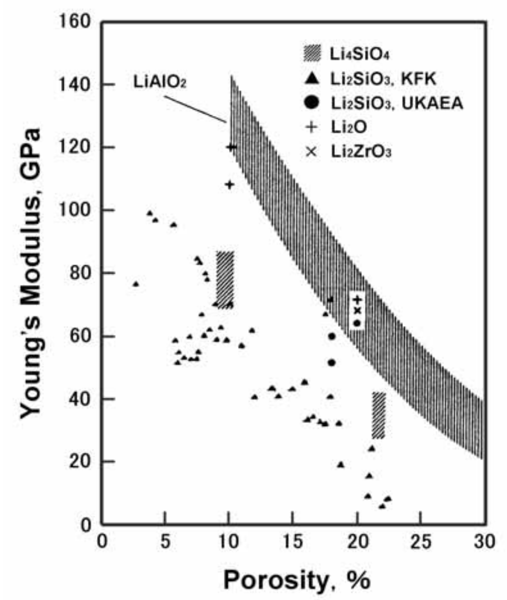

Fig.4.6 Porosity dependence of Young's Modulus values for Li_2O, Li_2ZrO_3 and Li_4SiO_4. [17) 6) 50)]

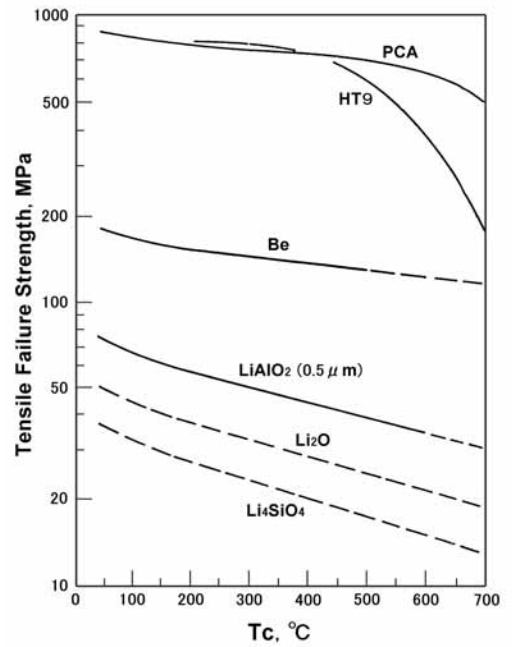

Fig.4.7 Calculated tensile failure strengths for 80% TD Li_2O, 80%TD Li_4SiO_4, Be, PCA and HT9. [16)]

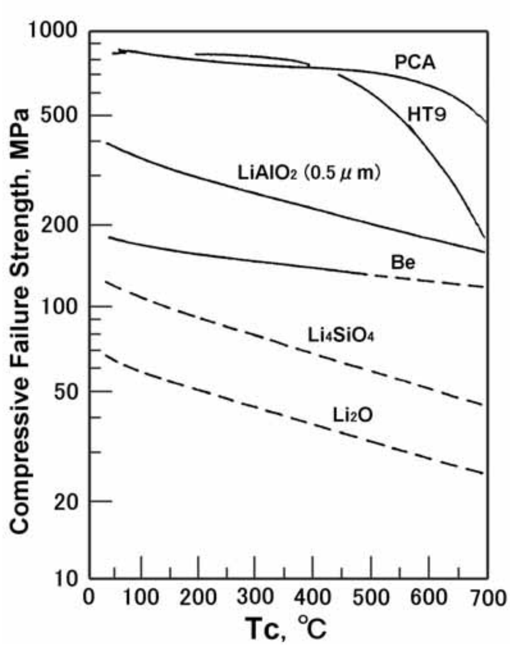

Fig.4.8 Calculated compressive failure strengths for 80% TD Li_2O, 80% TD Li_4SiO_4, Be, PCA and HT9. [16)]

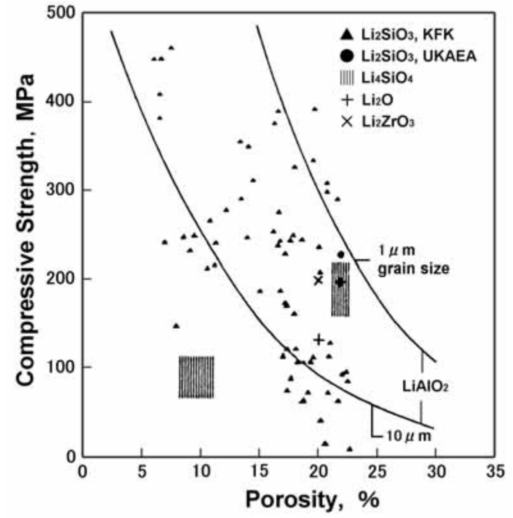

Fig.4.9 Porosity dependence of compressive strengths for Li_2O, Li_2ZrO_3 and Li_4SiO_4. [17)]

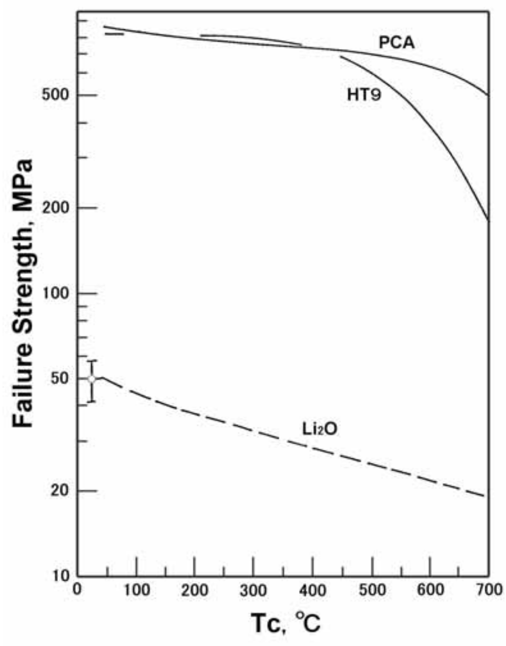

Fig.4.10 Bending failure strength for Li_2O (80% TD, 10 μm grain diameter). PCA and HT9 tensile failure strengths shown for reference purposes. [11)]

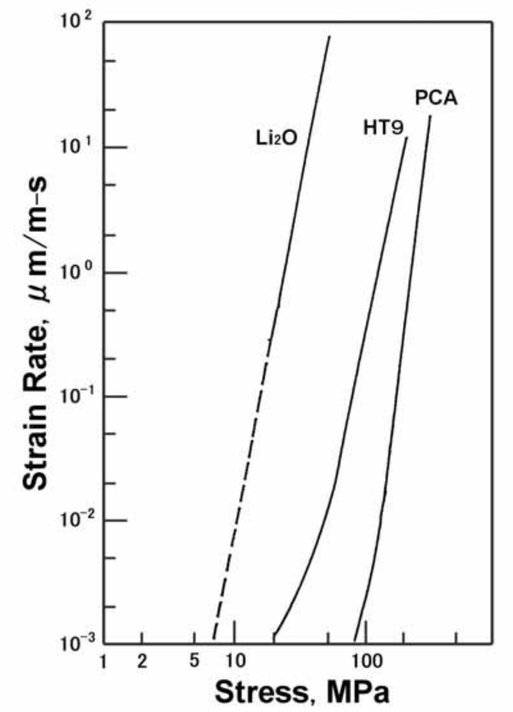

Fig.4.11 Secondary thermal creep rate for Li_2O (80% TD, 10 μm grain diameter) at 700℃. PCA and HT9 curves shown for reference purposes. [16)]

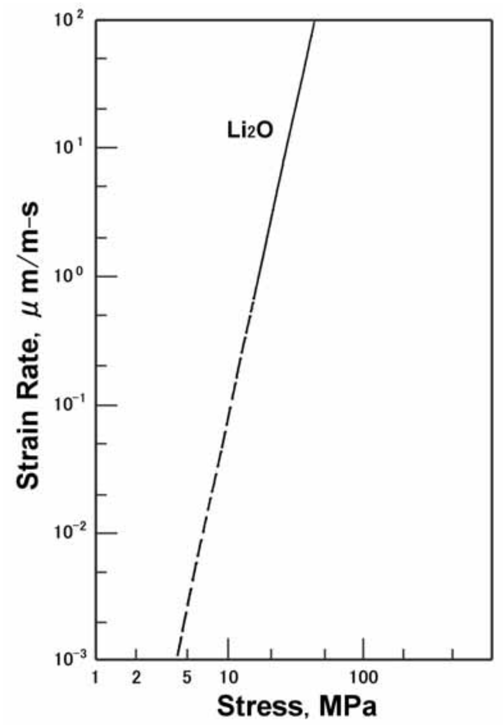

Fig.4.12 Secondary thermal creep rate for Li_2O (80% TD, 10 μm grain diameter) at 800℃. [16)]

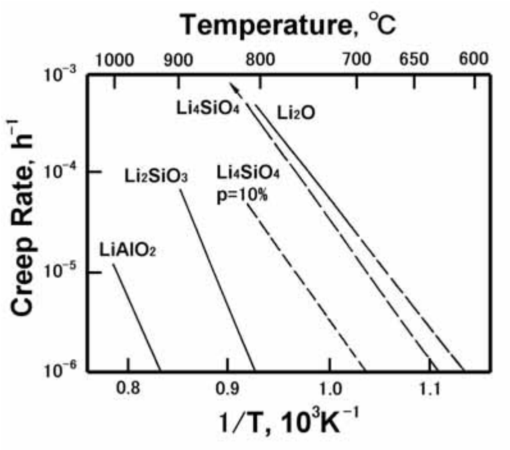

Fig.4.13 Compressive creep rates for Li_2O and Li_4SiO_4 (80% TD) (10MPa, 100h). [6]

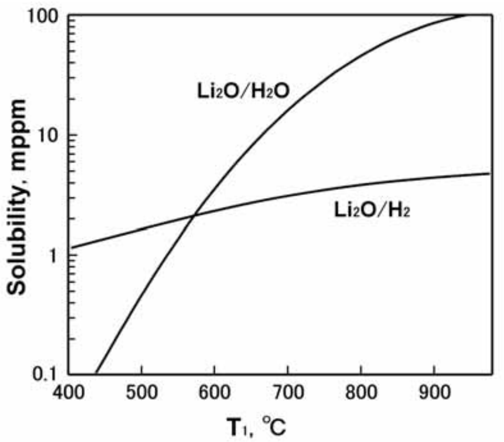

Fig.4.15 Hydrogen solubility in Li_2O at 10 Pa of H_2 or H_2O. [19) 39) 12]

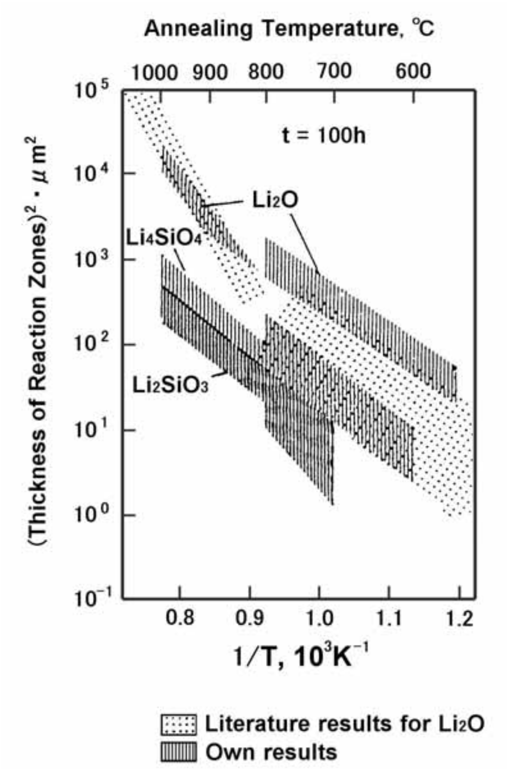

Fig.4.14 Chemical reaction between Li_2O and Li_4SiO_4 and structure materials during reaction time normalized to 100hr. [25]

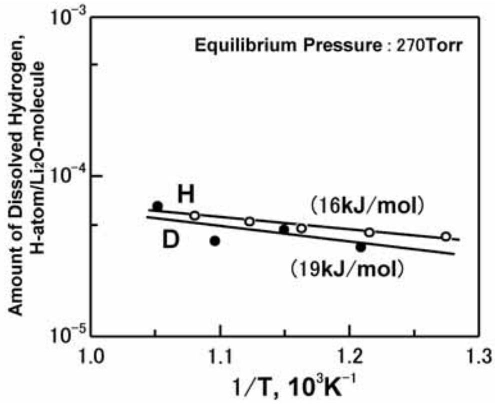

Fig.4.16 Temperature dependency of hydrogen and heavy hydrogen absorption for Li_2O. [30) 31]

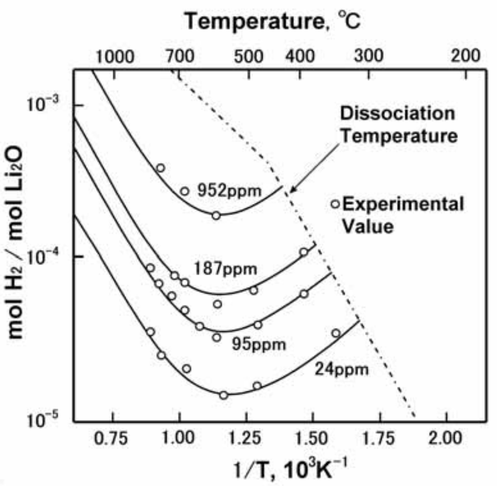

Fig.4.19 Water vapor adsorption to Li_2O. [32]

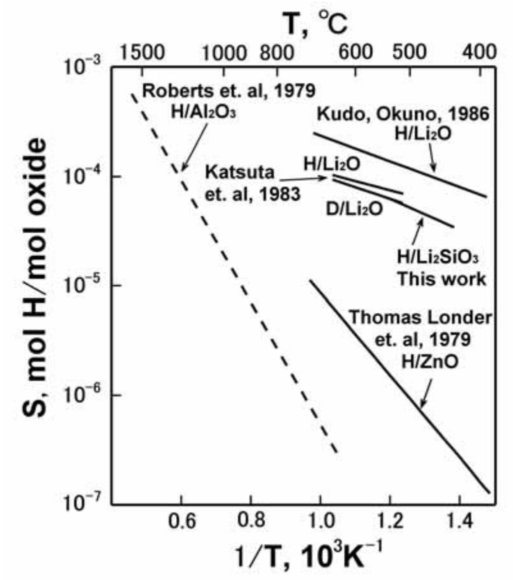

Fig.4.17 Hydrogen solubility in Li_2O. [31)]

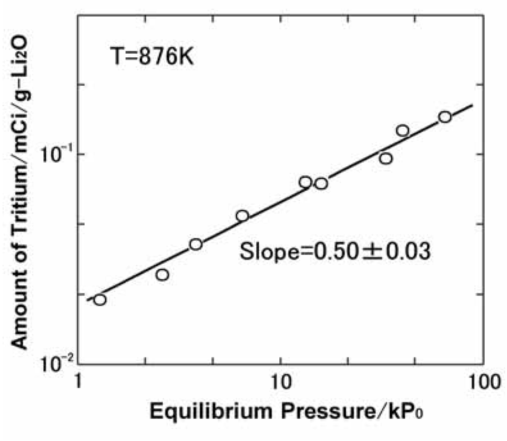

Fig.4.20 Tritium solubility in Li_2O crystal. [33)]

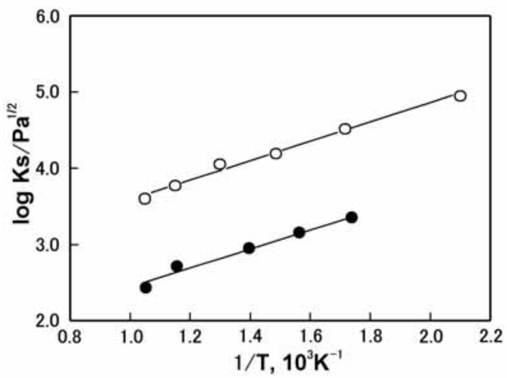

Fig.4.21 Hydrogen(○), Tritium(●), solubility in Li_2O. [14)]

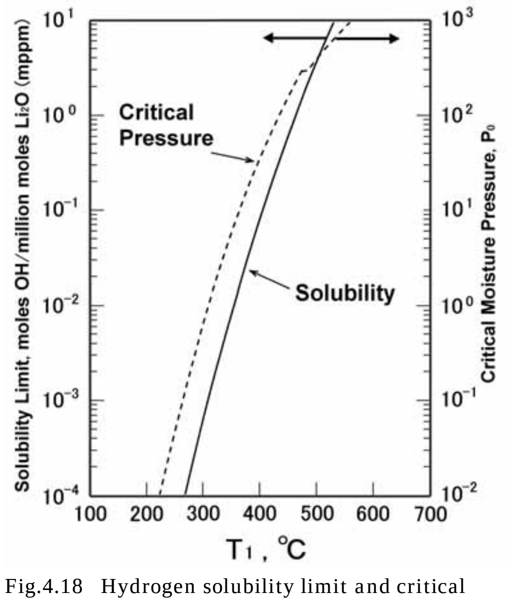

Fig.4.18 Hydrogen solubility limit and critical moisture pressure in Li_2O. [39)]

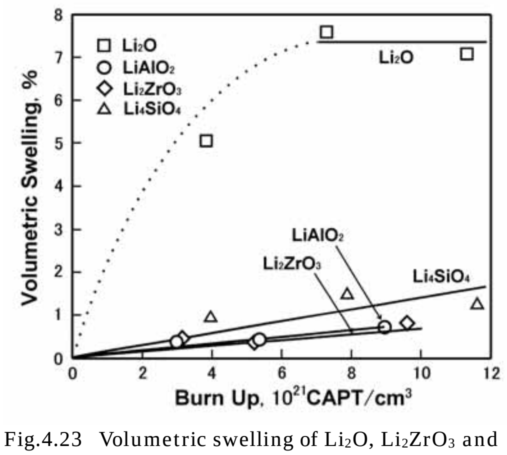

Fig.4.23 Volumetric swelling of Li_2O, Li_2ZrO_3 and Li_4SiO_4 at 700℃. [6) 49)]

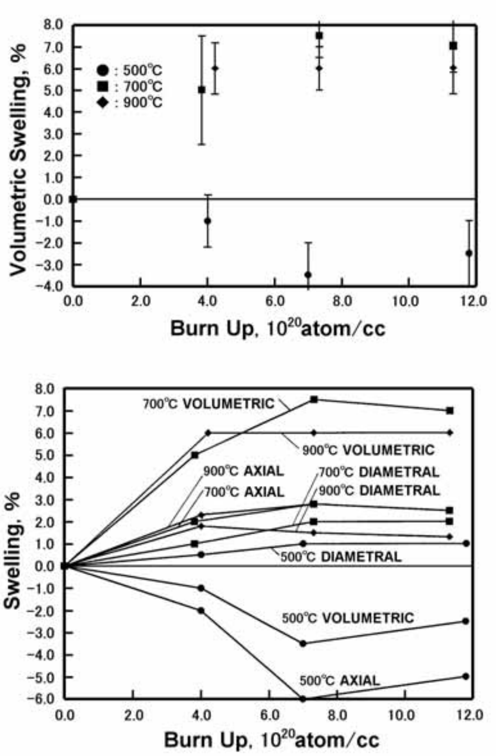

Fig.4.22 Relationship between burn up and swelling for Li_2O. 6) 30)

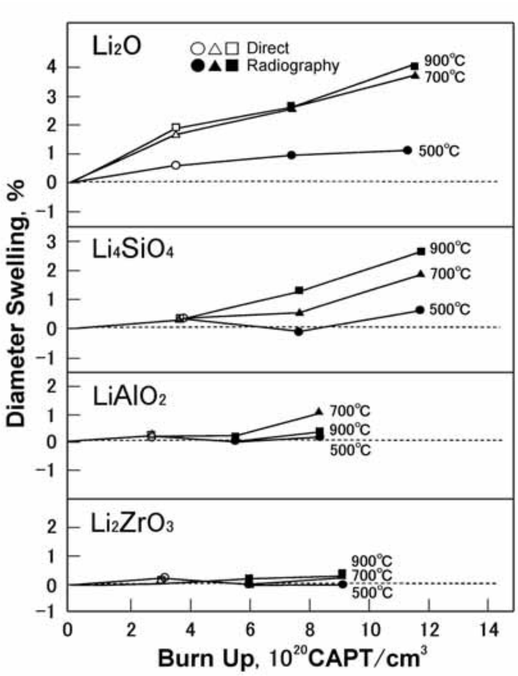

Fig.4.24 Diameter swelling of Li_2O, Li_2ZrO_3 and Li_4SiO_4 at 500℃, 700℃, 900℃. 6) 70)

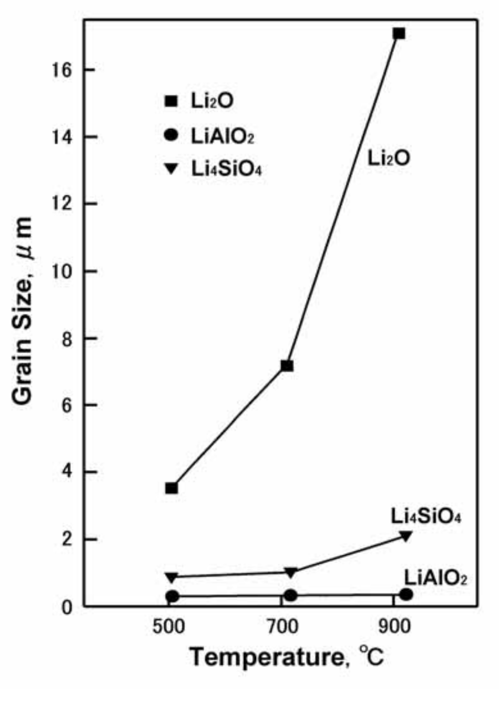

Fig.4.25 The grain size of irradiated Li_2O, Li_2ZrO_3 and Li_4SiO_4. The indicated grain size was determined by a linear intercept method, 100 full power days. (1% atom ^{6}Li burn-up). 36)

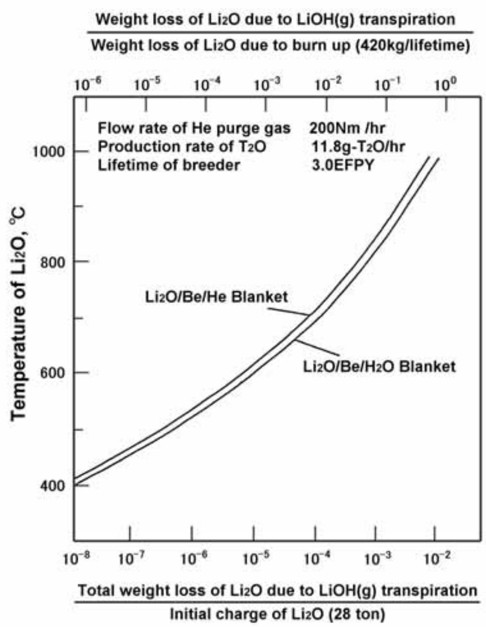

Fig.4.26 Relationship between weight loss of Li_2O and temperature. 37)

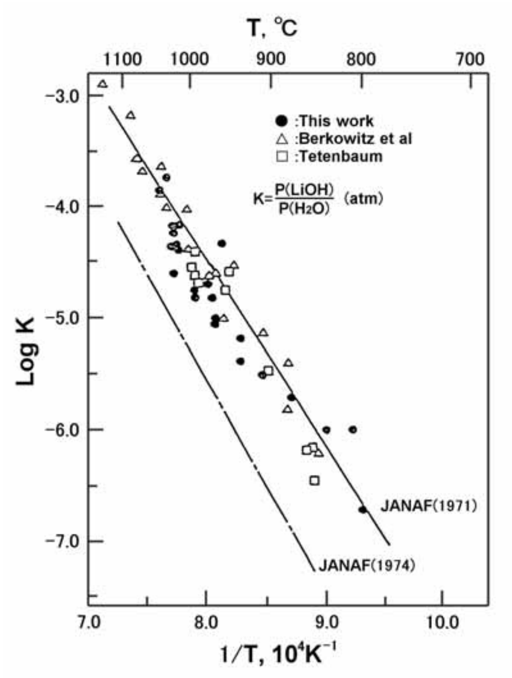

Fig.4.27 Equilibrium constant for the reaction $Li_2O(s) + H_2O = 2LiOH(g)$. [37)]

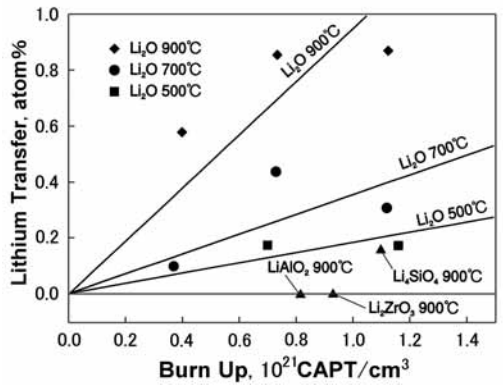

Fig.4.28 Burn up dependency of Li-transfer for Li_2O, Li_2ZrO_3 and Li_4SiO_4. [56)]

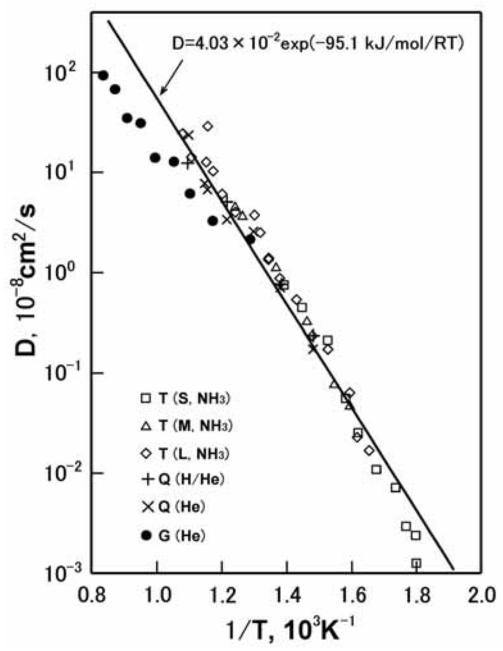

Fig.4.29 Lattice diffusion coefficient for lightly irradiated Li_2O from Tanifuji(T), Quanci(Q) and Guggi(G). [41)]

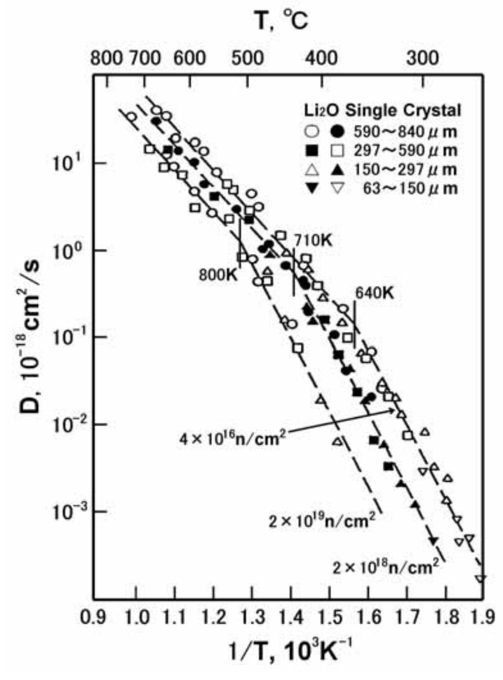

Fig.4.30 Lattice diffusion coefficient for Li_2O vs. fluence. [41)]

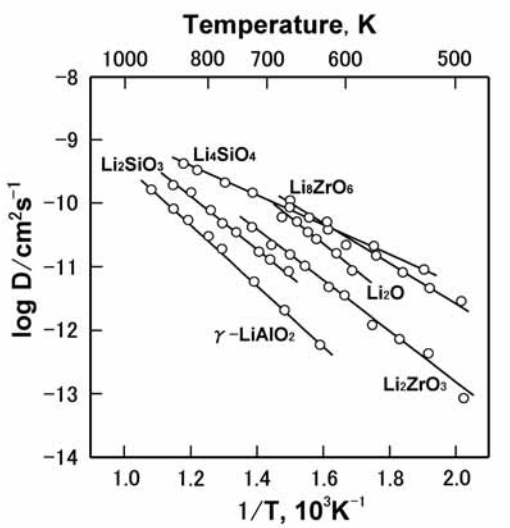

Fig.4.31 Diffusion coefficient of T in Li_2O, Li_2ZrO_3 and Li_4SiO_4. [33]

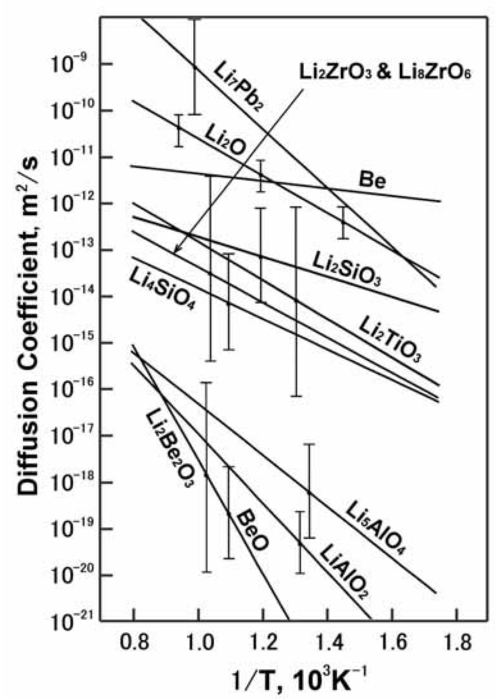

Fig.4.32 Summary of tritium diffusion coefficient in Li_2O, Li_2ZrO_3, Li_2TiO_3 and Li_4SiO_4. [18]

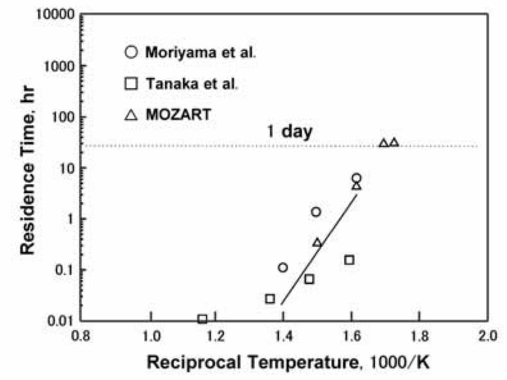

Fig.4.33 Tritium residence times for Li_2O. [47]

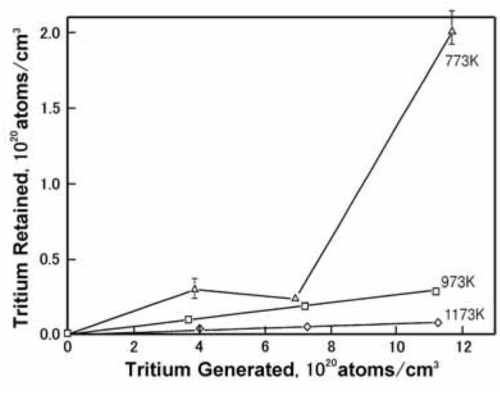

Fig.4.34 Tritium retention in Li_2O. [48]

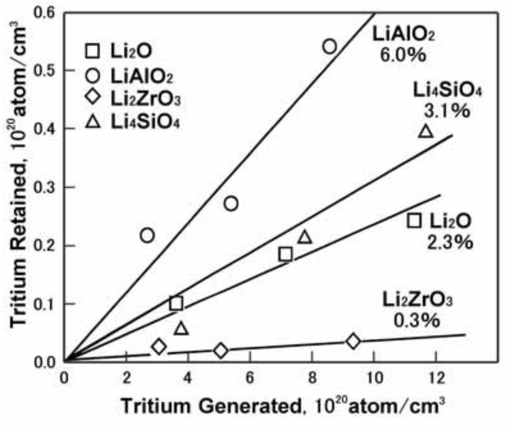

Fig.4.35 Tritium retention in Li_2O, Li_2ZrO_3 and Li_4SiO_4 at 700 ℃. [49]

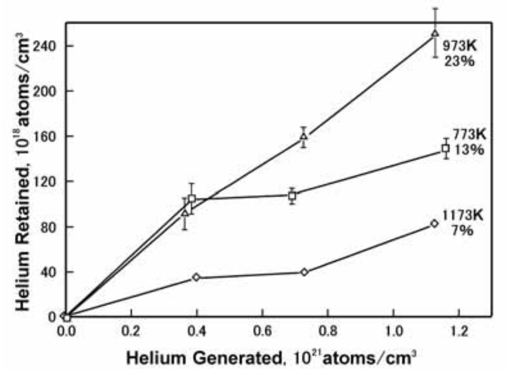

Fig.4.36 Helium retention in Li_2O. [48]

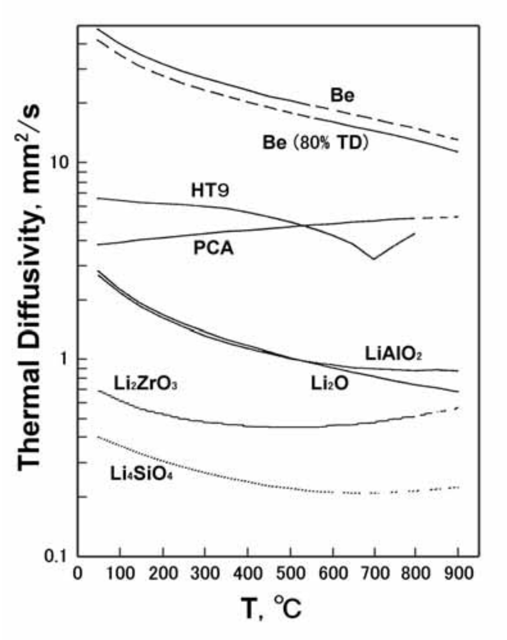

Fig.4.37 Thermal diffusivity of Li_2O, Li_2ZrO_3 and Li_4SiO_4 (80% TD). [12]